J Sol-Gel Sci Technol (2012) 62:208–216
DOI 10.1007/s10971-012-2711-0

ORIGINAL PAPER

Fabrication of a sol–gel derived microporous zirconia membrane for nanofiltration

Hong Qi · Guizhi Zhu · Li Li · Nanping Xu

Received: 19 August 2011 / Accepted: 2 February 2012 / Published online: 14 February 2012

Abstract This paper reports the fabrication and nanofiltration properties of a sol–gel derived microporous zirconia membrane. Effects of synthesis parameters, including hydrolysis time, hydrolysis temperature, hydrolysis ratio and chelating agent dopant, on the state and size of polymeric zirconia sol, were investigated. Highly reproducible and stable zirconia sol after refluxing at 40 °C for 180 min, with an average particle size of approximately 8.6 nm, was synthesized with a recipe of [Zirconium n-propoxide]: [Diethanolamine]: [1-propanol]: [H_2O] being 1: 2.2: 28.7: 9.4 (in molar ratio). The sol was subsequently used for the fabrication of microporous ZrO_2 membranes onto alumina supported mesoporous γ-Al_2O_3 layers. ZrO_2 membranes with molecular weight cut-off (MWCO) of 354, 1,195, corresponding to the pore size of 0.94 and 1.75 nm, were successfully fabricated. Ionic retention properties of such ZrO_2 membranes with respect to electrolyte solutions, like $MgCl_2$, $CaCl_2$, NaCl and Na_2SO_4, were also determined. Effects of parameters such as concentration of salt solutions and trans-membrane pressure on retention rates of microporous ZrO_2 membranes were studied in detail. Results showed that zirconium n-propoxide derived microporous ZrO_2 membranes exhibited comparatively high retention rates towards divalent ions like Mg^{2+} and Ca^{2+}, while much lower retention rates were observed for mono-valent ion (Na^+) in the present study, which are the characteristics of nanofiltration membranes.

H. Qi (✉) · G. Zhu · L. Li · N. Xu
State Key Laboratory of Materials-Oriented Chemical Engineering, Membrane Science and Technology Research Center, Nanjing University of Technology, Nanjing 210009, China
e-mail: hqinjut@yahoo.com.cn

Keywords Microporous membrane · Zirconia · Nanofiltration · Sol–gel · Diethanolamine

1 Introduction

As an environmental-friendly alternative to the conventional separation technologies, like distillation, extraction and adsorption, membrane-based separation processes have drawn a great deal of attention in recent two decades, due to their high energy efficiency and high performance [1]. Membranes are generally categorized into organic polymeric membranes and inorganic ones. Since their introduction to commercial applications in the early 1980s, owing to their thermal, chemical and mechanical stability under harsh conditions, ceramic membranes are making rapid progress in many areas such as food and beverage processing, biotechnology applications and water treatment [1–3]. Among these, ceramic membrane based microfiltration (with membrane pore size >50 nm) and ultrafiltration (with membrane pore size in the range of 2–50 nm) processes are most extensively applied. Due to its satisfied rejection properties towards multi-valent ions and removal of organic substances with molecular weight (MW) in the range of 200–1,000 g mol^{-1} [4], ceramic nanofiltration (NF) membranes (with pore size <2 nm) hold great promise for separation, refinement and condensation under extreme conditions where its polymeric counterpart cannot be used.

At present, much more investigations are focused on the development of ceramic NF membrane materials, including γ-Al_2O_3, TiO_2, ZrO_2 and HfO_2 [5–17], of which γ-Al_2O_3 and TiO_2 materials are most extensively studied. Alami-Younssi et al. [6] developed tubular γ-Al_2O_3 NF membranes with a pore size of 5 nm through sol–gel method

and reported its retention behaviour towards mineral salts. Schaep et al. [7] found that operation parameters, like salt concentration, trans-membrane pressure and solution pH, are of critical importance for retention properties of γ-Al_2O_3 NF membrane. Their results are interpreted by Donnan exclusion and double electrical layer theory. Topuz et al. [8] also fabricated γ-Al_2O_3 NF membrane through sol–gel route by tuning the processing parameters, including acidity, hydrolysis ratio and addition of the chelating agent. Van Gestal et al. [9, 10] investigated chemical stability of a γ-Al_2O_3 NF membrane. However, the lack of high enough chemical stability of γ-Al_2O_3 NF membrane severely limits its application under extreme pH conditions, which are often encountered in industrial processes. In comparison with γ-Al_2O_3, TiO_2 and ZrO_2 materials do exhibit much higher chemical stability and, hence, much research is focused on development of TiO_2 and ZrO_2 NF membranes. Van Gestal et al. [4] fabricated a TiO_2 NF membrane with a molecular weight cut-off (MWCO) lower than 600 and investigated its salt retention properties. Sekulic et al. [11] developed a TiO_2 NF membrane with a pore size of 0.8 nm by using a polymeric sol–gel technique. They demonstrated that strictly controlled processing parameters played an important role in obtaining polymeric titania sols providing low fractal dimensions. Xu et al. [12] synthesized unsupported TiO_2 and ZrO_2 xerogels, which are provided with an average pore diameter less than 2 nm and a microporosity more than 50%. Etienne et al. [13] fabricated a tubular ZrO_2 NF membrane exhibiting a retention rate of 90% towards a dextrane (MW = 10,000 g mol^{-1}). Vacassy et al. [14] developed an MgO-modified microporous ZrO_2 membrane, showing retention rates of 54 and 73% for saccharose (MW = 542 g mol^{-1}) and vitamin B_{12} (MW = 1,355 g mol^{-1}), respectively. Benfer et al. [15] observed that ZrO_2 NF membrane displayed a rejection rate as high as 66.3% with respect to SO_4^{2-}. Van Gestel et al. [16] fabricated disk ZrO_2 NF membranes with a MWCO lower than 300. Furthermore, long-term corrosion tests regarding this membrane demonstrated a good corrosion resistance under pH values of 13 and 1, respectively. Recently, Kreiter et al. [17] reported pervaporation and gas permeation performances of microporous ZrO_2 and TiO_2 membranes, which are fabricated through dip coating of nano-scaled zirconia and titania sols onto porous ceramic support.

With respect to metal alkoxide, it is well known that the hydrolysis reactivity increases in the order of cations Si≪Ti<Zr [18]. Consequently, in order to obtain polymeric ZrO_2 sol, the desired rate of hydrolysis reaction regarding zirconia alkoxide precursor must be controlled by adjusting various factors [19–22]. However, the systematical investigations on effects of synthesis parameters on the state and size of polymeric ZrO_2 sols are still scarce. On the other hand, the influence of the size and stability of the polymeric ZrO_2 sol on pore size of the ZrO_2 NF membrane is not clear yet. More important, although the retention properties of ZrO_2 NF membranes towards organic small molecules and electrolyte solutions (e.g. Na_2SO_4 and NaCl) are available [14, 23], more informations on retention properties of ZrO_2 NF membrane with regard to electrolyte solutions, are needed.

In this paper, we systematically studied the effects of synthesis parameters, including hydrolysis temperature, hydrolysis time, hydrolysis ratio and chelating agent dopant, on the state and size of zirconia n-propoxide derived sol. The stable nano-scaled polymeric ZrO_2 sol, with an average size of 8.6 nm, was used to fabricate ZrO_2 NF membrane through dip-coating approach. Pure water permeability and the MWCO of zirconia membranes were determined. The retention properties of such membranes with respect to electrolyte solutions, like $MgCl_2$, $CaCl_2$, Na_2SO_4 and NaCl, were also investigated in detail.

2 Experimental

2.1 Preparation of ZrO_2 polymeric sol

Polymeric ZrO_2 sol was prepared by using zirconium n-propoxide (70% in propanol, ABCR, hereafter denoted as ZnP) as a precursor. Diethanolamine (DEA) was used as a chelating agent to protect the ligands of zirconium n-propoxide, whose extremely high hydrolysis rate can be effectively reduced. To shed light on the effect of processing parameters on the state and the size of the ZrO_2 sol, recipes for the synthesis of ZrO_2 sols are listed in Table 1.

Table 1 Recipes for the synthesis of ZrO_2 sols

Number	Hydrolysis temperature (°C)	Hydrolysis time (min)	$[H_2O]/[ZnP]$ (molar ratio)	[DEA]/[ZnP] (molar ratio)
Sol-1	0	10	5.0	2.2
Sol-2	0	30	5.0	2.2
Sol-3	0	60	5.0	2.2
Sol-4	0	180	5.0	2.2
Sol-5	0	360	5.0	2.2
Sol-6	40	180	5.0	2.2
Sol-7	60	180	5.0	2.2
Sol-8	40	180	6.1	2.2
Sol-9	40	180	9.4	2.2
Sol-10	40	180	9.4	0
Sol-11	40	180	9.4	0.9
Sol-12	40	180	9.4	1.3
Sol-13	40	180	9.4	1.6
Sol-14	40	180	9.4	1.9

The general procedure for preparing a ZrO_2 polymeric sol was as follows. 4.5 mL ZnP was added into 20 mL 1-propanol. Then a certain quantity of DEA was drop-wise introduced into the ZnP solution under vigorous stirring. Both operations were carried out in nitrogen glove box. The mixture was subsequently placed into an ice bath to prevent premature hydrolysis. Deionized water was drop-wise added into the above-mentioned solution under vigorous stirring. The mixture was finally maintained at a fixed temperature for a certain period of time. The obtained polymeric ZrO_2 sol was cooled down to room temperature and diluted for 6 times with 1-propanol before dip-coating.

2.2 Fabrication of microporous ZrO_2 membrane

Supported microporous ZrO_2 membranes were fabricated through dip-coating the above-mentioned ***Sol-9*** onto home-made disk α-alumina supported mesoporous γ-alumina layers under clean room (class 1000) conditions. After that, ZrO_2 membranes were calcined under air at 350 and 400 °C for 3 h (hereafter referred to as Zr-350 and Zr-400, respectively), with heating and cooling rates of both 0.5 K min^{-1}.

2.3 Characterization

Effective particle sizes in the polymeric ZrO_2 sols were measured by dynamic light scattering (DLS) using a Zetatrac analyser (Microtrac Inc.). Pure water permeability of disk membrane was characterized by using a dead-end filtration apparatus under trans-membrane pressure in the range of 0.3–0.7 MPa, as shown in Fig. 1. The pure water permeability was calculated with Eq. 1 as follows.

$$Q = \frac{m}{\rho A t \Delta p} \quad (1)$$

where Q is the membrane permeability (L m^{-2} h^{-1} MPa^{-1}), m is the weight of the permeate (kg), A is the effective filtration area (m^2), t is the filtration time (h), Δp is the trans-membrane pressure (MPa), and ρ is the density of the permeate solution (kg dm^{-3}).

Retention properties of membrane Zr-350 and Zr-400 were characterized by a dead-end filtration mould using the same apparatus, as depicted in Fig. 1, while the feed solution was kept stirring at a speed of 200 r min^{-1} to avoid concentration gradient. The feed solution contained PEGs (Alfa Aesar) with molecular masses of 200, 600, 1,500, and 4,000, while the concentration was 3 g L^{-1}. The measurements were conducted at a trans-membrane pressure of 0.76 MPa and a temperature of 25 ± 2 °C. The retention rates of the membrane were determined with gel permeation chromatography (GPC, Waters), by collecting both feed and permeate solutions. The molecular mass of the PEG corresponding to a 90% retention level was taken as the MWCO (molecular weight cut-off) of the membrane.

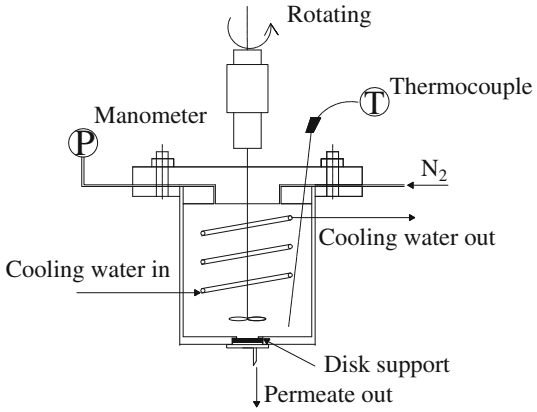

Fig. 1 Schematic diagram of dead-end filtration apparatus

Nanofiltration properties of microporous ZrO_2 membranes (Zr-350 and Zr-400), characterized as its ionic retention properties at ambient temperature (25 ± 2 °C), were determined by using the same filtration apparatus under trans-membrane pressures in the range of 0.4–0.8 MPa, as shown in Fig. 1. The feed solution was kept stirring at a speed of 200 r min^{-1} to avoid concentration gradient. Ionic retention properties of microporous ZrO_2 membranes (Zr-350 and Zr-400) towards single component salt solutions, like $MgCl_2$, $CaCl_2$, Na_2SO_4 and NaCl, were conducted by using the same apparatus shown in Fig. 1. The concentration and pH value of above-mentioned salt solutions was controlled in the range of 0.005–0.1 mol L^{-1} and 6.0 (tuned by addition of HNO_3 and NH_3 H_2O), respectively. Ionic retention rates of microporous ZrO_2 membranes were determined by measuring conductivities of salt solutions, which were collected from both feed and permeate side, and calculated with Eq. 2 as follows.

$$R(\%) = \left(1 - \frac{C_{ip}}{C_{if}}\right) \times 100. \quad (2)$$

where R is the ionic retention rate of the membrane, C_{ip} is the ionic concentration of permeate solution, C_{if} is the ionic concentration of feed solution.

3 Results and discussion

3.1 Effects of processing parameters on properties of polymeric ZrO_2 sols

Polymeric ZrO_2 sol prepared by using zirconium n-propoxide as a precursor generally consists of hydrolysis reaction and condensation reactions, as shown in Eqs. 3–5,

respectively, through which branched polymeric particles consisting of Zr–O–Zr bonds can be formed.

$$Zr(OR)_4 + H_2O \rightarrow Zr(OR)_3(OH) + ROH \quad (3)$$

$$Zr(OR)_3(OH) + Zr(OR)_3(OH) \rightarrow (RO)_3Zr - O - Zr(OR)_3 + H_2O \quad (4)$$

$$Zr(OR)_3(OH) + Zr(OR)_4 \rightarrow (RO)_3Zr - O - Zr(OR)_3 + ROH \quad (5)$$

where R represents C_3H_7.

It is reported that acetylacetone, diethanolamine and acetic acid can be used to modify zirconium alkoxide precursors [15, 20], so as to obtain polymeric ZrO_2 sols rather than precipitates or gels. In this study, effect of DEA doping on zirconium n-propoxide derived sols state as well as its particle sizes, was investigated. Figure 2 shows the effect of the amount of DEA dopant on the state of ZrO_2 sols. As can be seen in Fig. 2a, white precipitate was instantaneously formed once the water was drop-wise introduced into the ZnP precursor solution with the absence of DEA additive, indicating the hydrolysis reaction proceeds much faster than the condensation one. The result corroborates that the extremely high hydrolysis rate of the zirconium alkoxide precursor is one of the main hurdles to synthesis transparent polymeric ZrO_2 sol containing mainly branched polymeric particles, as also observed by Gu et al. [24]. White jelly was gradually formed during the water addition, which indicates polymeric ZrO_2 sol still cannot be obtained if the doping DEA amount was low (e.g. molar ratio for DEA to ZnP (hereafter referred to as [DEA]/[ZnP]) was less than 1.0), as evidenced in Fig. 2b. Figure 2c shows that clear and transparent sol can be obtained as the doping amount of DEA increased, regardless of the hydrolysis time (maximum hydrolysis time is 360 min in this study). Figure 3 displays the particle size distributions of transparent ZrO_2 sols synthesized with the [DEA]/[ZnP] in the range of 1.3–2.2. It can be seen in Fig. 3 that the average particle size of sol decreased with [DEA]/[ZnP], from 12.3 ([DEA]/[ZnP] = 1.3) to 8.9 nm ([DEA]/[ZnP] = 2.2). Meanwhile, the particle size distribution of

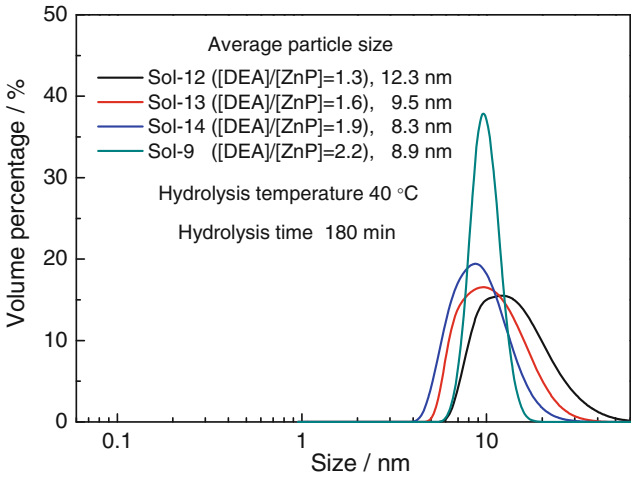

Fig. 3 Particle size distributions of ZrO_2 sols as a function of the amount of DEA dopant ([DEA]/[ZnP] was in the range of 1.3–2.2)

the sol became narrower, as also observed in Fig. 3. It is worthwhile to note that the sol size did not vary too much when the ratio of [DEA]/[ZnP] is greater than 1.5.

Hydrolysis time is one of the most important parameters to synthesis polymeric sol. Taking into account that the high hydrolysis rate of zirconium alkoxide precursors, synthesis of ZrO_2 polymeric sol was conducted in an ice bath (maintained at 0 °C) to study the effect of hydrolysis time on sol properties. Figure 4 gives the particle size distributions of zirconia sols as a function of hydrolysis time. It can be seen that a short hydrolysis time (e.g. 10 min) resulted in a comparatively wide size distribution in the range of 1–10 nm, with an average size of approximately 1.8 nm. All the ZrO_2 sols exhibited narrow particle size distributions in the range of 1–3 nm, with a mean particle size of around 1.5 nm, irrespective of hydrolysis time. It should also be noted that all sols were clear and transparent even if the hydrolysis time was as long as 360 min. As is well known that the apparent size of the sol particles is relevant to the fabrication of microporous membranes. Under water depletion conditions the sol–gel reaction primarily yields linear, lightly branched polymer

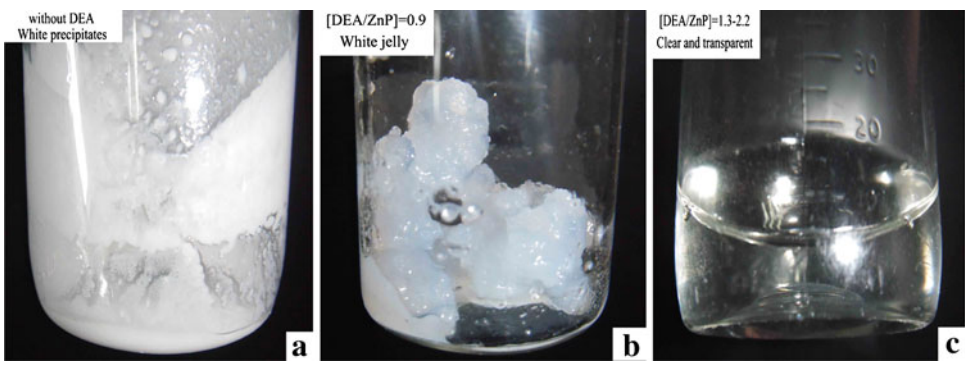

Fig. 2 Effect of the amount of DEA dopant on the state of polymeric ZrO_2 sols (**a** without DEA; **b** [DEA]/[ZnP] = 0.9; **c** [DEA]/[ZnP] = 1.3–2.2)

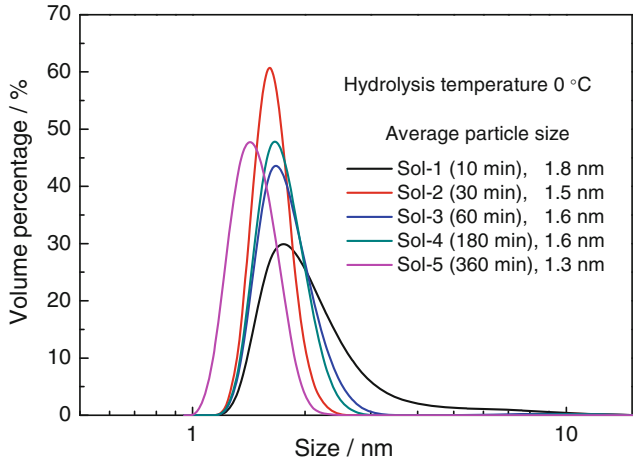

Fig. 4 Particle size distributions of ZrO_2 sols as a function of hydrolysis time (hydrolysis and condensation were carried out in ice bath)

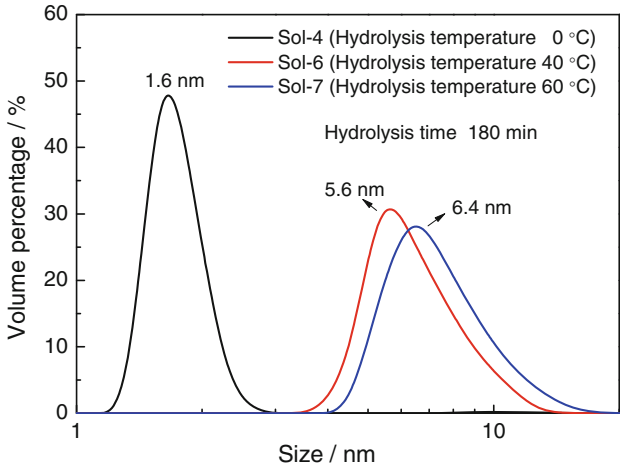

Fig. 5 Particle size distributions of ZrO_2 sols as a function of hydrolysis temperature

particles, which entangle inducing gelation during deposition of the sol on a porous ceramic support. The size of the sol particles displayed in Fig. 4 is considered relatively small and will lead to excessive penetration of the polymer particles into the γ-alumina mesoporous support layer (with pores 5–6 nm). It is widely accepted that the hydrolysis reaction of metal alkoxide can be accelerated with increased hydrolysis temperature [21]. Therefore, ZnP precursor solution refluxing at higher temperatures was carried out to find whether highly branched polymer particles can be formed. Figure 5 gives the particle size distributions of ZrO_2 sols as a function of hydrolysis temperature. All the ZrO_2 sols exhibited clear and transparent appearance after hydrolysis for 180 min. However, larger sol size as well as wider size distribution can be obtained when the hydrolysis temperature elevated, as shown in Fig. 5. Similar results were also observed in Ref. [25]. When the hydrolysis and condensation reactions underwent at 40 and 60 °C, the apparent ZrO_2 sol size was 5.6 and 6.4 nm, respectively. The size of the sol particles displayed in Fig. 5 is considered large enough to prevent excessive penetration of the polymer particles into the γ-alumina mesoporous support layer (with pores 5–6 nm) and, hence, might be suitable for the subsequent formation of microporous ZrO_2 membranes.

It is well known that hydrolysis ratio has a decisive effect on the average particle size of metal alkoxide derived sol. Figure 6 presents the particle size distributions of ZrO_2 sols as a function of hydrolysis ratio ($[H_2O]/[ZnP]$). As shown in Fig. 6, the average particle size of ZrO_2 sol gradually increased with hydrolysis ratio, from 5.7 ($[H_2O]/[ZnP] = 5$) to 8.9 nm ($[H_2O]/[ZnP] = 9.4$). The result can be attributed to the accelerated hydrolysis reaction rate caused by the addition of more water. With

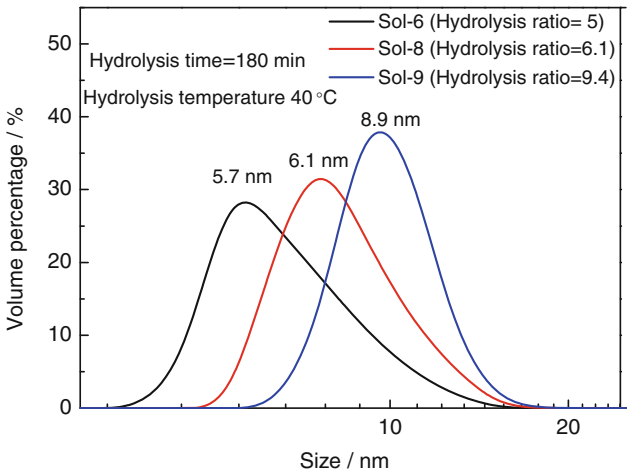

Fig. 6 Particle size distributions of polymeric ZrO_2 sols as a function of hydrolysis ratio (hydrolysis and condensation were carried out at 40 °C)

respect to the sol size for microporous membranes fabrication, Van Gestel et al. [26] found that the microporous ZrO_2 membrane, fabricated by using a ZrO_2 sol with an average particle size of 6 nm, was impermeable for water under a trans-membrane pressure as high as 1.0 MPa, indicating a completely dense membrane structures. The results also indicate that the relationship between the sol size and the membrane pore size is still not clear. Considering that the hydrolysis ratio of 5.0 and 6.1 might not yield suitable ZrO_2 sol for dip-coating because of its relative small particle size, the hydrolysis ratio of 9.4 was preferably chosen for sol synthesis and further membrane fabrication.

Based on the above-mentioned results, ZrO_2 ***Sol-9*** (with a recipe of [ZnP]: [DEA]: [propanol]: $[H_2O]$ = 1: 2.2: 28.87: 9.4, in molar ratio) synthesized at 40 °C for 180 min

was suitable for dip-coating because of its appropriate average particle size (8.9 nm) and comparatively narrow particle size distribution. Taking into account that the reproducibility as well as stability of polymeric ZrO_2 sol plays a vital role on fabrication of microporous ZrO_2 membranes, synthesis of ZrO_2 ***Sol-9*** was reproduced for three times, with the results shown in Fig. 7. It can be seen in Fig. 7 that three batches of ***Sol-9*** show similar particle size distribution, with an average particle size of ca. 8.6 nm, which indicates a satisfying reproducibility. The Storage of ZrO_2 ***Sol-9*** under −2 °C over 3 months entailed no apparent change of the particle size distribution, while the sol was still clear and transparent (see Fig. 8). The sol maintained at an average size of 7.7 nm even after storage over 3 months, indicating that lightly branched polymeric chains retained in the ZrO_2 sol, which is of great importance for the subsequent deposition on porous ceramic support. Consequently, ***Sol-9*** was chosen for the fabrication of microporous ZrO_2 membranes through dip-coating approach.

3.2 Retention properties of microporous ZrO_2 membranes

3.2.1 Pure water permeability and MWCO of microporous ZrO_2 membranes

Pure water permeability and PEG retention property of zirconia membranes (Zr-350 and Zr-400) are displayed in Figs. 9 and 10, respectively. As can be seen in Fig. 9, the pure water flux of membranes increased linearly as the pressure increased, with the pure water permeability of

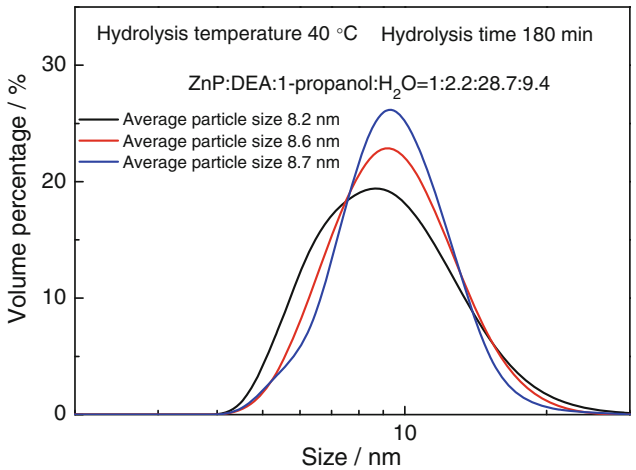

Fig. 7 Particle size distributions of ZrO_2 ***Sol-9*** reproduced for 3 times

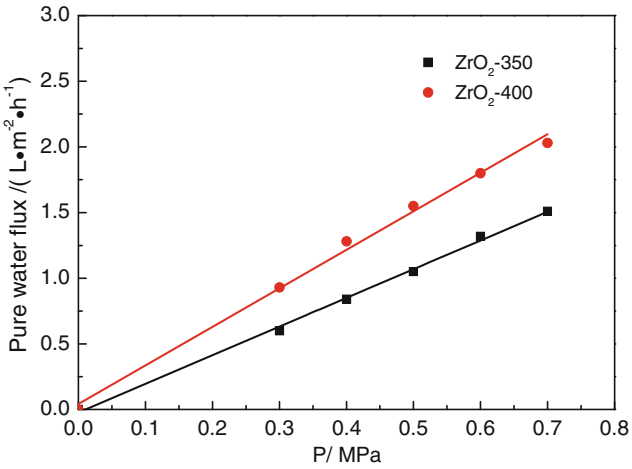

Fig. 9 Pure water permeability of ZrO_2-350 and ZrO_2-400 membranes

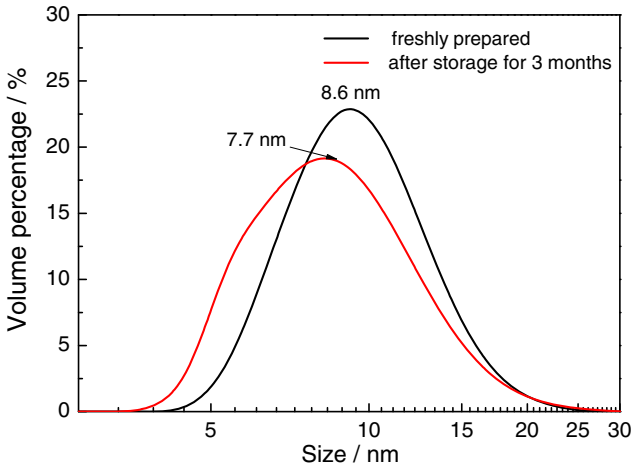

Fig. 8 Particle size distributions of freshly prepared ZrO_2 ***Sol-9*** and that after storage under −2 °C over 3 months

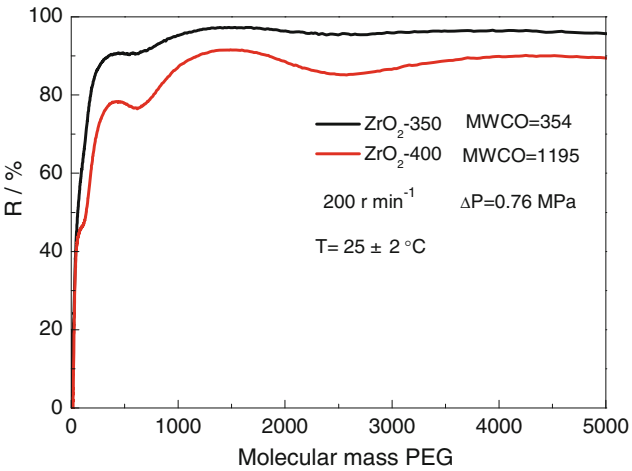

Fig. 10 PEG retention properties of ZrO_2-350 and ZrO_2-400 membranes

membranes was in the range of 2–3 L/(m^2 h MPa). It can be observed in Fig. 10 that the MWCO of membrane Zr-350 and Zr-400 was 354 and 1,195, corresponding to the pore size of 0.94 and 1.75 nm respectively, based on the calculation with Eq. 6 [27].

$$R(\text{Å}) = 0.262 \times (M_W)^{0.5} - 0.3 \quad (6)$$

where R (Å) is the pore radius of the membrane, M_W is the MWCO of the membrane.

3.2.2 *Ionic retention properties of microporous ZrO_2 membranes*

Ionic retention properties of Zr-350 and Zr-400 membranes with respect to single component salt, like $CaCl_2$, $MgCl_2$, NaCl and Na_2SO_4, are displayed in Figs. 11 and 12, respectively. As can be seen in both figures, the ionic retention rate decreased as the salt concentration increased. These results can be explained by the variation of thickness of the double electronic layer formed in the membrane pores during the contact of the membrane with salt solutions [4, 7, 28]. Skluzacek et al. [28] reported that a larger thickness of the double electronic layer presented in the membrane would provide a higher potential at the center of the membrane pores and, hence, results in a higher retention rate towards salt solutions. The thickness of the double electronic layer presented in the membrane can be characterized by the Debye length λ_D, and represented as Eq. 7 [7]

$$\lambda_D = \left(\frac{\varepsilon_0 \varepsilon_r RT}{F^2 \sum_i z_i^2 c_i} \right)^{1/2} \quad (7)$$

where λ_D is the Debye length (m), ε_0 is the permittivity of vacuum (8.85×10^{-12} C V^{-1} m^{-1}), ε_r is the relative permittivity (78.3 for water at 25 °C), R is the universal gas

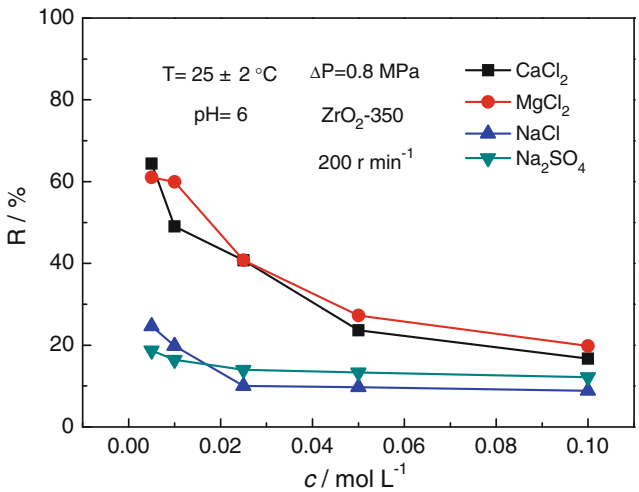

Fig. 11 Ionic retention properties of microporous ZrO_2 membrane (ZrO_2-350) as a function of salt concentration

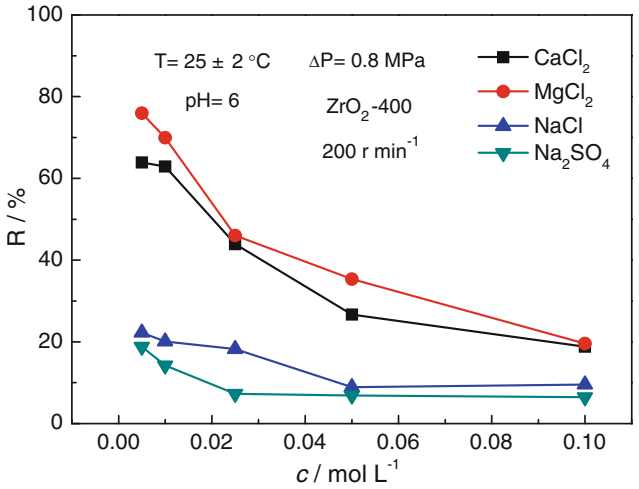

Fig. 12 Ionic retention properties of microporous ZrO_2 membrane (ZrO_2-400) as a function of salt concentration

constant (8.314 J mol^{-1} K^{-1}), T is the temperature (K), F is the Faraday' constant (96,487 C mol^{-1}), Z_i is the valence of ion i, c_i is the ion concentration (mol m^{-3}).

Table 2 presents the Debye length as a function of the concentration of salt solutions studied in this paper. It can be seen in Table 2 that the higher the concentration (i.e. with higher ionic strength) of the salt solutions, the smaller the thickness of the double electronic layer will be, which is responsible for the lower retention rate of microporous ZrO_2 membranes. Therefore, a decreased salt concentration results in a higher retention. It should be noted that the salt retention rate of Zr-400 membrane was in the following sequence as R ($MgCl_2$) > R ($CaCl_2$) > R (NaCl) > R (Na_2SO_4), which is the characteristic of positively charged NF membranes [14, 29]. These observations can be explained by the charging effects and sieving effects [30, 31]. Table 3 displays the basic parameters of ions studied in this paper. As can be seen in Table 3, both ionic radius and hydrated radius of cations and anions are much smaller than the membrane pore size (1–2 nm), which indicates sieving effects could not lead to the effective retention of ions, as observed in Figs. 11 and 12. The ions retention property was mainly influenced by the membrane charging effects. As schematic shown in Fig. 13a [6], the presence

Table 2 Debye lengths (nm) of salts with various concentrations

Salt concentration (mol L^{-1})	Debye length (nm)	
	NaCl	Na_2SO_4/$CaCl_2$/$MgCl_2$
0.005	4.29	2.48
0.01	3.04	1.75
0.025	1.92	1.11
0.05	1.36	0.78
0.1	0.96	0.55

Table 3 Basic parameters of ions studied in this paper [31–33]

Ions	Ionic radius (nm)	Hydrated radius (nm)	Hydration energy (kJ mol^{-1})	Diffusion coefficient (10^{-9} m^2 s^{-1}) (at 25 °C)
Mg^{2+}	0.072	0.428	1,921	0.7
Ca^{2+}	0.099	0.412	1,577	1.14
Na^{+}	0.102	0.358	295	1.35
Cl^{-}	0.181	0.332	376	2.03
NO_3^{-}	0.189	0.340	329	–
SO_4^{2-}	0.24	0.300	1,138	1.05

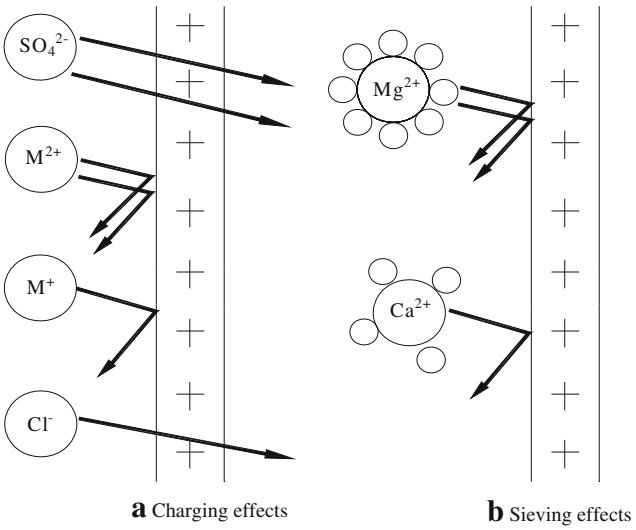

Fig. 13 Schematic diagram of rejection mechanism for positive nanofiltration membranes [6]

of repulsive force between the membrane and di-valent co-ions (M^{2+}) is stronger than that with mono-valent co-ions (Na^{+}). Meanwhile, counter-ions weaken this repulsive force and, hence, leads to the retention sequence of R ($CaCl_2$, $MgCl_2$) > R (NaCl) > R (Na_2SO_4). On the other hand, the higher retention rate for the membrane towards Mg^{2+} than that was found for Ca^{2+}, can also be explained by the hydration pattern of the ions. It is reported that hydration pattern is characterized by the ion sizes, which means well hydrated ions will be rejected more efficiently than poorly hydrated ones [6], depending on their hydration energy. Taking into account that the hydration energy of Mg^{2+} (1,921 kJ mol^{-1}) is higher than that of Ca^{2+} (1,577 kJ mol^{-1}) [31, 32], the magnesium ion is more readily hydrated than calcium ion and, hence, giving rise to a higher rejection of $MgCl_2$. Schematic diagram for the retention mechanism can be found in Fig. 13b [6]. The retention rates of Zr-350 membrane towards salt solutions showed the same variation tendency as that found for Zr-400 membrane, as illustrated in Fig. 11. It was found

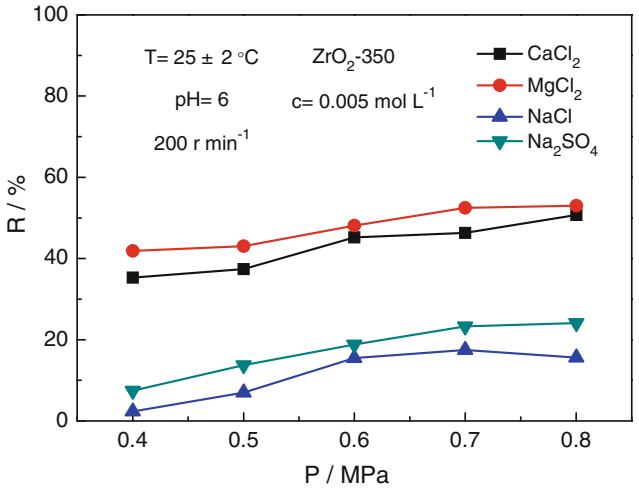

Fig. 14 Ionic retention properties of microporous ZrO_2 membrane (ZrO_2-350) as a function of trans-membrane pressure

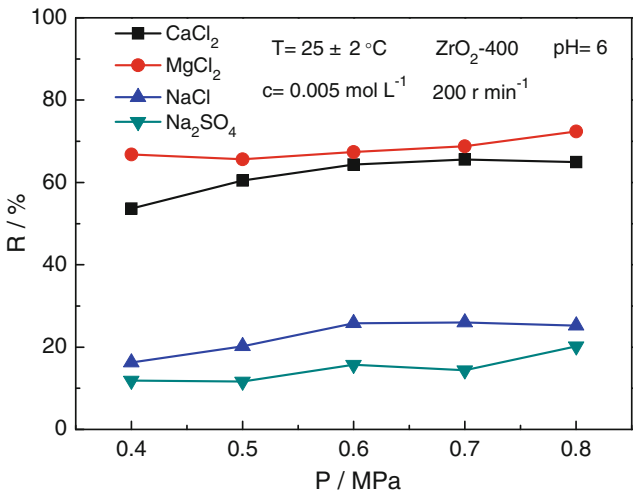

Fig. 15 Ionic retention properties of microporous ZrO_2 membrane (ZrO_2-400) as a function of trans-membrane pressure

that sol–gel derived ZrO_2 membranes exhibited comparatively high retention rates towards Mg^{2+} (76%) and Ca^{2+} (64%), while much lower retention rate was noticed for mono-valent ion of Na^{+} (<20%) in this study.

Figures 14 and 15 present the salt retention rate of Zr-350 and Zr-400 membranes as a function of trans-membrane pressure with respect to single component salt solutions of $CaCl_2$, $MgCl_2$, NaCl and Na_2SO_4. As can be seen in both figures, the salt retention rate increased with the pressure up to 0.6 MPa and then reached an asymptotic value. Ions transport through the membrane is determined by diffusion (due to a concentration gradient), convection (due to a pressure gradient) and electromigration (due to an electrical potential gradient) mechanisms [27]. At lower trans-membrane pressures, diffusion has a major influence

on the ions transport, leading to a lower retention rate. At high trans-membrane pressures, effect of the diffusion mechanism on the membrane retention can be neglected, while both convection and electromigration mechanisms affect the ions transport and, hence, giving rise to a constant retention rate. On the other hand, the retention rates of Zr-350 and Zr-400 membranes with respect to $MgCl_2$ was higher than that found for $CaCl_2$, can also be explained by diffusion mechanism of the ion transport through membranes [34]. As is known that the diffusion coefficient of Mg^{2+} (0.7×10^{-9} m^2 s^{-1} at 25 °C) is lower than that of Ca^{2+} (1.14×10^{-9} m^2 s^{-1} at 25 °C) [32, 33], the higher retention rate of the membrane towards Mg^{2+} is expected if taking account of the reverse relationship between diffusion velocity of ions and membrane retention rate [35].

4 Conclusion

Clear and transparent polymeric ZrO_2 sols were prepared through accurately controlled hydrolysis and condensation of zirconium n-propoxide precursor doped with diethanolamine. The state and size of zirconium sols are dependent on hydrolysis time, hydrolysis temperature, hydrolysis ratio and molar ratio of [DEA]/[ZnP]. With a recipe of [ZnP]: [DEA]: [1-propanol]: $[H_2O] = 1: 2.2: 28.7: 9.4$, a polymeric ZrO_2 sol with an average particle size of 8.6 nm can be synthesized under a refluxing temperature of 40 °C for 180 min. Storage at −2 °C over 3 months entailed no apparent change of the particle size, while the sol was still clear and transparent. Microporous zirconia membranes can be fabricated by using such nano-scaled polymeric ZrO_2 sol via dip-coating approach, followed by calcination at both 350 and 400 °C. Sol–gel derived microporous ZrO_2 membranes exhibited comparatively high retention rates towards di-valent ions like Mg^{2+} (76%) and Ca^{2+} (64%), while much lower retention rate was found for mono-valent ion Na^+ (<20%) in this study, which are the characteristics of nanofiltration membranes.

Acknowledgments The authors would like to thank the financial support from the National Natural Science Foundation of China (20906047), the Natural Science Research Plan of Jiangsu Universities (11KJB530006), the "Summit of the Six Top Talents" Program of Jiangsu Province and State Key Laboratory of Materials-Oriented Chemical Engineering (ZK201002).

References

1. Richard WB (2004) Membrane technology and applications. Wiley, Menlo Park
2. Vander Bruggen B, Mänttäri M, Nyström M (2008) Sep Purif. Technol 63:251–263
3. Weber R, Chmiel H, Mavrov V (2003) Desalination 157:113–125
4. Van Gestel T, Vandecasteele C, Buekenhoudt A, Dotremont C, Luyten J, Leysen R, Van der Bruggen B, Maes G (2002) J Membr Sci 209:379–389
5. Blanc P, Larbot A, Palmeri J, Lopez M, Cot L (1998) J Membr Sci 149:151–161
6. Alami-Younssi S, Larbot A, Persin M, Sarrazin J, Cot L (1995) J Membr Sci 102:123–129
7. Schaep J, Vandecasteele C, Peeters B, Luyten J, Dotremont C, Roels D (1999) J Membr Sci 163:229–237
8. Topuz B, Çiftçioğlu M (2010) J Sol-Gel Sci Technol 56:287–299
9. Van Gestel T, Vandecasteele C, Buekenhoudt A, Dotremont C, Luyten J, Leysen R, Van der Bruggen B, Maes G (2002) J Membr Sci 207:73–89
10. Van Gestel T, Vandecasteele C, Buekenhoudt A, Dotremont C, Luyten J, Van der Bruggen B, Maes G (2003) J Membr Sci 214:21–29
11. Sekulic J, Ten Elshof JE, Blank DHA (2004) J Sol-Gel Sci Technol 31:201–204
12. Xu QY, Anderson MA (1994) J Am Ceram Soc 77:1939–1945
13. Etienne J, Larbot A, Julbe A, Guizard C, Cot L (1994) J Membr Sci 86:95–102
14. Vacassy R, Guizard C, Thoraval V, Cot L (1997) J Membr Sci 132:109–118
15. Benfer S, Popp U, Richter H, Siewert C, Tomandl G (2001) Sep Purif Technol 22–23:231–237
16. Van Gestel T, Kruidhof H, Blank DHA, Bouwmeester HJM (2006) J Membr Sci 284:128–136
17. Kreiter R, Rietkerk MDA, Bonekamp BC, Van Veen HM, Kessler VG, Vente JF (2008) J Sol-Gel Sci Technol 48:203–211
18. Pierre AC (1999) Introduction to sol-gel processing. Kluwer, Boston
19. Ju XS, Huang P, Xu NP, Shi J (2000) J Membr Sci 166:41–50
20. Wu JCS, Cheng LC (2000) J Membr Sci 167:253–261
21. Larry LH, Jon KW (1990) Chem Rev 90:33–72
22. Tsuru T (2008) J Sol-Gel Sci Technol 46:349–361
23. Benfer S, Árki P, Tomandl G (2004) Adv Eng Mater 6:495–500
24. Gu YF, Kusakabe K, Morooka S (2001) Sep Sci Technol 36:3689–3700
25. Kreiter R, Rietkerk MDA, Castricum HL, Veen HM, ten Elshof JE, Vente JF (2011) J Sol-Gel Sci Technol 57:245–252
26. Van Gestel T, Sebold D, Kruidhof H, Bouwmeester HJM (2008) J Membr Sci 318:413–421
27. Puhlfürß P, Voigt A, Weber R, Morbé M (2000) J Membr Sci 174:123–133
28. Skluzacek J, Tejedor M, Anderson M (2007) J Membr Sci 289:32–39
29. Ryan JN, Elimelech M, Baeseman JL, Magelk RD (2000) Environ Sci Technol 34:2000–2005
30. Ballet GT, Hafiane A, Dhahbi M (2007) J Membr Sci 290:164–172
31. Paugam L, Taha S, Dorange G, Jaouen P, Quéméneur F (2004) J Membr Sci 231:37–46
32. Tansel B, John S, Tony R, Jay G, Richard FS, Lanfang L, Michael R, Mary H, Jan B (2006) Sep Purif Technol 51:40–47
33. Rios GM, Joulie R, Sarrade SJ, Carlès M (1996) AIChE J 42:2521–2528
34. Chaudhari LB, Murthy ZVP (2010) J Hazard Mater 180:309–315
35. Murthy ZVP, Chaudhari LB (2009) Chem Eng J 150:181–187